Rheo-viscoelastic behavior and viscosity prediction of calcium sulphoaluminate modified Portland cement pastes

Y.M. Peng[a, b], *C. Unluer*[a], *J.Y. Shi*[b, *]

[a] School of Engineering, University of Glasgow, Glasgow G12 8LT, United Kingdom

[b] School of Civil Engineering, Central South University, Changsha 410075, PR China

[*] School of Civil Engineering, Central South University, Changsha 410075, PR China

Highlights:

- A model to predict the η_{min} by PC and CSA volume fractions is proposed.
- PC and CSA increase the η_{min}, critical strain and flow strain of paste.
- The proposed η_{min} prediction model has high accuracy at both 5 min and 60 min.
- The accuracy of prediction model at 5 min is higher than that at 60 min.

Abstract: In this study, the rheo-viscoelastic behaviors of calcium sulphoaluminate (CSA) modified Portland cement (PC) pastes were investigated. The shear stress, apparent viscosity, frequency sweep and time sweep curves of composite pastes with different PC and CSA volume fractions were analyzed, and the minimum apparent viscosity (η_{min}) of PC-CSA pastes were predicted. Results show that with the increase of PC and CSA volume fractions, η_{min}, critical strain and flow strain of pastes increase at both 5 min and 60 min resting time, and the phase angle varies under different time spots. The accuracy of viscosity prediction models for 5 min and 60 min are both relatively high. Meanwhile, the reason why the prediction accuracy of 5 min is higher than 60 min is that with

the prolongation of resting time, the relationships between particle volume fractions and rheological properties are affected by the early microstructure formed by flocs and hydration products, thus affecting their original functional relationship at 5 min.

Keywords: Portland cement, calcium sulphoaluminate cement, minimum apparent viscosity, viscoelasticity, viscosity prediction model

1 Introduction

With the development of cement industry, it has gradually become an effective method to improve specific properties of cement mixes by mixing with other kinds of mineral admixtures or clinkers. Among them, calcium sulphoaluminate (CSA) modified Portland cement (PC) is considered as a kind of compound cement with great potential and prospect due to its advantages of combination of both PC and CSA clinkers [1].

Owing to the high production of carbon dioxide and large consumption of energy in the process of cement clinker calcination, reducing the utilization of cement clinker has important practical significance for energy saving and environmental protection. CSA clinker can be made of limestone, calcium sulfate and alumina as well as some industrial by-products or wastes, leading to its lower CO_2 emission per gram of clinker than that of alite, which is a main component of PC clinker [2-4]. The maximum calcination temperature of CSA is 200°C lower than PC clinker, and CSA clinker is easy to grind compared with PC [5, 6]. Furthermore, CSA cement also has the characteristics of high early strength development rate and shrinkage compensation [7]. From these points of view,

PC-CSA mixes has great development potential. Many researchers have carried out relevant researches on fresh and hardened properties of PC-CSA mixes [8-9]. After incorporating CSA, the setting time of cement paste decreases [8]. CSA clinker plays an important role in early mechanical properties, while OPC is mainly responsible for hardened strength [9]. Meanwhile, curing temperature is critical to the hydration process of CSA cement. Different curing temperature will not change the type of hydration products of CSA cement, but will affect its quantity [10]. In terms of raw materials for the production of CSA clinker, Shen et al. [11] studied the potential of using phosphogypsum (PG) to produce CSA cement and the decomposition behavior of PG in CSA cement production, and the results showed that PG can be used to produce CSA cement, and the effect of PG decomposition on the formation of CSA is significant. In addition, the incorporation of mineral admixtures and chemical admixtures can also affect CSA cement or PC-CSA cement. The early strength and setting time of CSA can be significantly enhanced by lithium carbonate-aluminum sulfate at 0 ℃ [12]. At the same time, lithium carbonate aluminum-sulfate not only promoted the formation of ettringite, but also accelerated the hydration of C_2S. Zhang et al. [13] found that the addition of excessive retarder will reduce the activity of CSA cement particles and contribute to the decline of compressive strength. Fu et al. [14] pointed out that burnt plaster and alunite can control the decrease of long-term strength of sulphoaluminate cement, and they can also improve its resistance to drying contract and chemical correlation.

Rheological properties of fresh cementitious materials not only have an important impact on the construction process, but also are closely related to the hardened performances [15]. Rheological properties are the intrinsic properties of concrete workability, and rheology of cement paste largely dictates rheology of concrete, especially at early ages [16, 17]. For the Bingham model, the two

most important basic parameters are plastic viscosity and yield stress [18, 19]. Besides the properties of fluid, cement paste will show certain elastic properties when subjected to different amplitude or frequency of external shear force, which is described as the term "viscoelasticity" [20, 21]. With the continuous hydration of cement, the paste gradually loses its fluidity, sets and hardens into a semi-solid or solid-phase system dominated by elasticity [22, 23]. Rheological properties and viscoelasticity (rheo-viscoelastic properties) summarize the change process of the physical state of paste from fresh stage to setting and hardening stage. The addition of several additives can also affect the rheological properties of PC or CSA paste. Hydroxypropyl methylcellulose could significantly increase the stress and viscosity of sulphoaluminate cement paste [24]. The hydration rate and compressive strength of CSA mixes were improved after the incorporation of ettringite seed crystals, while yield stress, plastic viscosity and setting time was on the decline [25].

CSA modified PC pastes have excellent properties of both PC and CSA. Despite many researches have focused on the effects of mineral or chemical admixtures on rheology of PC or CSA mixes, there are still few comprehensive studies on the rheo-viscoelastic of PC-CSA composite pastes. Considering that there is also no relevant viscosity prediction analysis for this system, in this study the rheo-viscoelastic behavior is comprehensively analyzed by means of dynamic rheological test, amplitude sweep and time sweep, and then the prediction model of the minimum apparent viscosity (η_{min}) under the resting time of 5 min and 60 min was given. Finally, based on the viscoelasticity test within 60 min, the reasons for the difference in the prediction accuracy of viscosity under different resting time were discussed.

2 Materials and methods

2.1 Materials and mixture proportions

Commercial Portland cement (PC) P·I 42.5 (conforming to GB 8076) and calcium sulphoaluminate cement (CSA) were provided by China Building Materials Academy. The density of PC and CSA is 3.15 g/cm^3 and 2.80 g/cm^3 respectively. Their chemical composition and some physical properties are shown in **Table 1**, and particle size distribution is presented in **Fig. 1**. Polycarboxylate superplasticizer (PCE) with water-reducing rate 32% and solid content 33.1% was used to disperse fresh composite pastes.

The mixture proportions of PC-CSA systems are displayed in **Table 2**. In order to improve the accuracy of prediction, here the mixed PC and water are regarded as a solvent, while CSA is considered as a solute to predict the viscosity of PC-CSA-H_2O paste (**Fig. 2**). According to the mass ratio of **Table 2**, when the volume ratio $\varphi_C/(\varphi_C+\varphi_W)$ (abbreviated as $\varphi_{C/W}$) is between 0.45 and 0.6, the water-to-binder ratios (*W/B*) of composite pastes incorporating less than 20wt % CSA range from 0.15 to 0.4. Because some of mix proportions have very low *W/B* ratio and a certain volume of flocculation structure exists in the fresh pastes, which may affect the relationship between particle volume fraction and viscosity, a sufficient amount of PCE was added into each paste to disperse the flocs and ensure the homogeneity of paste. The process of mixing pastes was first mixing at 60 rpm for 60 s, then stopped for 30 s, and finally mixing at 120 rpm for 60 s.

2.2 Rheological test

2.2.1 Dynamic test

An Anton Paar MCR 102 rheometer was used to measure the rheology of different pastes. The height (H) of 4-blade vane rotor was 40 mm, and the internal radius (R_1) and outer radius (R_2) were

11 mm and 21 mm respectively. The external cylinder remained stationary during rheological test.

The rheological test protocol is shown in **Fig. 3**. The test started at 5 min after the initial contact of water, PC and CSA, and the test was conducted again after 60 min. First, a 60 s pre-shear at 100 s^{-1} were intended to create a uniform condition. After resting for 60 s, the shear rate increased logarithmically from 1 s^{-1} to 100 s^{-1} in 100 s, and the time interval between two test points was 2 s. The typical rheological curves of pastes are shown in **Fig. 4**. It is found that with the increase of shear rate, the rheological behavior will change from shear thinning to shear thickening. This shear rate is called critical shear rate (γ_{crit}), and the corresponding shear stress and viscosity can be described as critical shear stress (τ_{crit}) and η_{min} [26]. When the apparent viscosity of paste reaches the minimum, the volume of flocculation structure is relatively small and the relationship between the volume fraction and rheological properties is significant. Therefore, the aim of this study is to predict the η_{min} of composite pastes with particle volume fractions of PC and CSA.

2.2.2 Amplitude sweep test

The goal of amplitude sweep is to measure the change of viscoelasticity with strain. In oscillation test, the rotor oscillates along the axis at a set frequency. Here the frequency was kept constant at 1 Hz, while the strain was increased logarithmically from 10^{-3} % to 10^{2} % in 0 s~200 s (**Fig. 5**). The test was carried out at 10 min after the contact of clinker and water. The variation of some viscoelastic parameters with amplitude can be obtained by amplitude sweep test, such as G', G'' and δ. The relationships among these parameters are as follows [20]:

$$G' = \frac{\sigma_0 \cos\delta}{\varepsilon_0} \tag{1}$$

$$G'' = \frac{\sigma_0 \sin\delta}{\varepsilon_0} \tag{2}$$

$$\tan\delta = \frac{G''}{G'} \quad (3)$$

Where G' is storage modulus, G'' is loss/viscous modulus, σ_0 is stress, δ is phase angle and ε_0 is strain. In these parameters, G' characterizes the elastic behavior of paste, while G'' characterizes the viscous behavior.

2.2.3 Time sweep test

The change of viscoelasticity with time due to the evolution of paste internal microstructure can be investigated by time sweep test. In this study, the same frequency (1 Hz) as the amplitude sweep was adopted, and the results of amplitude sweep showed that for PC-CSA system, when the amplitude was controlled within 10^{-4} %, both G' and G'' were relatively stable, and the internal structure of fresh paste had not been significantly damaged, so the amplitude value was determined to be 10^{-4} %. G'' and G' were measured every 30 s for 60 min, and the phase angle δ was calculated by the tangent of G''/G'.

3 Results and discussion

3.1 Rheo-viscoelastic behavior

3.1.1 minimum apparent viscosity

Fig. 6 give the change of η_{min} with different PC and CSA particles volume fraction (i.e. $\varphi_{C/W}$ and φ_S). The change in η_{min} were tested over 60 min after the initial contact of binders with water. The changing trend reveals that η_{min} depends not only on $\varphi_{C/W}$ and φ_S, but also relates to resting time. As seen from **Fig. 6**, the incorporation of CSA dramatically increases the η_{min} at both 5 min and 60 min resting time. The viscosity of composite pastes increases with increasing φ_S ranging from 0 to 0.2. Furthermore, with the increase of $\varphi_{C/W}$, η_{min} of composite pastes also increases gradually. The η_{min} of PC-CSA pastes with $\varphi_{C/W}$=0.45 and $\varphi_{C/W}$=0.5 are very close. However, when $\varphi_{C/W}$ rises to

0.55, the viscosity increases significantly. When the particle volume fraction reaches a certain degree, the rate of contact between particles and the formation of microstructure such as flocculation and initial hydration products are accelerated, which may significantly increase the yield stress and viscosity of cement pastes [27]. Compared with 5 min, the η_{min} of composite pastes under the same $\varphi_{C/W}$ and φ_S is larger at 60 min resting time.

3.1.2 Amplitude sweep

Viscoelasticity is an important property to characterize the change of internal structure of pastes. **Fig. 7** presents the typical curves of G', G'' and their evolutions with strain, and the viscoelastic parameters of pastes with different PC and CSA volume fraction are summarized in **Table 3**. Generally, if the test sample has a yield point, the G' which represents the elastic behavior plays a dominant role in small deformation. In a certain deformation range, the two moduli can be kept at a constant level, which is independent of the set amplitude and frequency. This range of reversible elastic deformation is also known as the linear viscoelastic region (LVR) [28]. Then G' and G'' are no longer constant and begins to decline, which correspond to the critical strain. When G' and G'' curves intersect, the amplitude at the intersection of storage modulus and loss modulus can be regarded as the flow point. When the applied strain is larger than this critical value, the microstructure of paste will be destroyed irrecoverably. According to the variation of viscoelastic parameter, it can be found that when $\varphi_{C/W}$ and φ_S increases, the values of G' and G'' corresponding to the critical amplitude and the critical strain/flow point strain all increase. The wider the range of LVR is, the larger amplitude is needed to destroy the network structure of colloidal particles in pastes, showing its stronger ability to resist external deformation. The addition of CSA densifies the internal structure and make the pastes difficult to be disassembled.

3.1.3 Time sweep

Fig. 8 illustrates the changing trend of G', G'' and δ over time. Regardless the volume fraction of PC and CSA, all pastes present similar results, that is, G' and G'' increased with increasing resting time. For C45-S0 paste, the value of G' is greater than G'' within the first 50 min. δ fluctuates in the first 30 min, and then increases with the prolongation of resting time after 30 min. When the volume fraction of CSA increase (**Fig. 8(b)**), G' and G'' are higher than that of C45-S0 paste at the same time point, and the two moduli are not intersected within 60 min. The decreasing rate of δ is more obvious in the first 20 min, and the increasing rate is comparatively small in the next 40 min.

3.2 Viscosity prediction

3.2.1 Methodology for predicting the viscosity

For rheological properties of cement suspension, the volume fraction of particles is a major determinant affecting its viscosity. It is generally considered that there is certain functional relation between suspension viscosity and particle volume fraction [29]. PC-CSA paste can be regarded as a suspension incorporating PC and CSA particles. Due to the differences in physicochemical properties of PC and CSA, their viscosity characteristics before and after mixing together vary significantly. Therefore, the viscosity of composite paste should be characterized by the volume fraction of PC particles ($\varphi_{C/W}$) and the volume fraction of CSA particles (φ_S) respectively. The basic prediction function is shown in Eq. (4):

$$\eta = \eta_0 \cdot f(\varphi_{C/W}, \varphi_S) \tag{4}$$

where η is the viscosity of composite paste, η_0 is the viscosity of suspension medium (water). Although the above function expression gives the method to predict viscosity by using $\varphi_{C/W}$ and φ_S respectively, the result of one-time analysis of multivariate function expression is generally not

accurate enough. In this study, the volume fraction of PC is larger than that of CSA, so the composite paste can be regarded as CSA suspended in PC-H_2O system. Therefore, the Eq. (4) can be rewritten as Eq. (5) and Eq. (6):

$$\eta = \eta_C \cdot f(\varphi_S) \tag{5}$$

$$\eta_C = \eta_0 \cdot f(\varphi_{C/W}) \tag{6}$$

where η_C is the viscosity of PC suspension. According to Eq. (5) and Eq. (6), the prediction of PC-CSA pastes viscosity can be divided into two steps: (1) $f(\varphi_{C/W})$ is predicted from the viscosity of pure cement paste and water. (2) $f(\varphi_S)$ is predicted from the viscosity of PC-CSA pastes and cement paste with the same PC volume fraction. Furthermore, according to the viscosity test results of **Fig. 6**, CSA particles have greater impact on viscosity than PC particles. Therefore, the viscosity prediction parameter $f(\varphi_{C/W})$ of PC with the characteristics of small viscosity influence and large volume fraction at 5 min and 60 min was first calculated, and then the CSA viscosity parameter $f(\varphi_S)$ was computed.

3.2.2 Prediction of $f(\varphi_{C/W})$

In this study, the PC particle volume fractions of all pastes are more than 45%, belonging to high concentration suspension. Krieger and Dougherty [30] have proposed a model which can well predict the viscosity of various high concentration suspensions, and the equation is as follows:

$$\eta_r = \left(1 - \frac{\varphi}{\varphi_m}\right)^{-K} \tag{7}$$

Where η_r is the relative viscosity (in this part, $f(\varphi_{C/W})$). φ and φ_m is the actual volume fraction of particles and maximum particle packing density respectively. K is a fitting parameter. It can be found from Eq. (7) that φ_m and K are two unknown parameters. Liu [31] found that the linear relationship between $1-\eta_r^{-1/2}$ and φ can be obtained by transforming the above expression when K=2. Based on

the above consideration, Liu modified the above function expression and added an adjustment coefficient. The modified expression is as follows:

$$\eta_r = [b(1-\frac{\varphi}{\varphi_m})]^{-2} = [a(\varphi_m - \varphi)]^{-2} \quad (8)$$

Where $a=b/\varphi_m$. Rearranging the terms in Eq. (8), leads to Eq. (9) as:

$$1-\eta_r^{-1/2} = 1-a\varphi_m + a\varphi \quad (9)$$

Fig. 9 shows the value of a and φ_m calculated by Eq. (9) when the correlation coefficient R^2 reach the maximum. It can be seen in **Fig. 9** that R^2 is greater than 0.8 in both 5 min and 60 min, indicating the fitting accuracy is relatively high. Therefore, it is feasible to use Eq. (9) to predict $f(\varphi_{C/W})$. The prediction functions of PC paste at 5 min and 60 min are shown in Eq. (10) and Eq. (11):

5 min:

$$f(\varphi_{C/W}) = [0.097*(0.9144-\varphi_{C/W})]^{-2} \quad (10)$$

60 min:

$$f(\varphi_{C/W}) = [0.0689*(1.0377-\varphi_{C})]^{-2} \quad (11)$$

3.2.3 Prediction of $f(\varphi_S)$

Compared with PC, the volume fraction of CSA particle is much smaller and the values of φ_S in this study are no more than 20%. For the suspension system with relatively small concentration, some models can be used to predict the viscosity by volume fraction. Among them, one of the widely used models is Einstein model [32]:

$$\eta_r = \frac{\eta}{\eta_0} = 1+2.5\varphi \quad (12)$$

Where η_r is the relative viscosity (the ratio of the suspension viscosity to the dispersion medium

viscosity). However, this model is basically applicable to the case where φ tends to zero. There are other models that can be used to calculate the relative viscosity by particle volume fraction. The two most frequent models are Batchelor model [33] and Brinkman model [34], which is shown in Eq. (13) and Eq. (14):

$$\eta_r = 1 + 2.5\varphi + 6.2\varphi^2 \tag{13}$$

$$\eta_r = \frac{1}{(1-\varphi)^{2.5}} \tag{14}$$

Among them, Batchelor model is based on Einstein model and takes Brownian motion into account. Meanwhile, since the Brinkman model is derived by adding more particles into the diluted suspension to increase the viscosity, it can be applied to suspensions with higher concentration than Einstein model. When φ is very small, Brinkman model can be simplified to Eq. (15):

$$\eta_r = \frac{1}{1-2.5\varphi} \tag{15}$$

All the above models can predict the viscosity by the volume fraction of suspension particles. However, these models do not consider the effect of particles water film thickness in the suspension [35-37]. The existence of adsorbed water layer will make the actual volume fraction of particles in the suspension larger than the calculated particle volume fraction. Assuming that the particles in the suspension are spherical, the actural volume fraction k can be obtained by Eq. (16):

$$k = (1 + \frac{r}{R})^3 \tag{16}$$

Where R and r are the diameters of suspension particle and water film thickness respectively. Considering the influence of adsorbed water layer, an unknown parameter k can be added to the above viscosity prediction model:

$$\text{Einstein model: } \eta_r = (1 + 2.5k\varphi) \tag{17}$$

Batchelor model: $\eta_r = 1 + 2.5k\varphi + 6.2(k\varphi)^2$ (18)

Brinkman model: $\eta_r = \frac{1}{(1-k\varphi)^{2.5}}$ (19)

Simplified Brinkman model: $\eta_r = \frac{1}{1-2.5k\varphi}$ (20)

These four models are adopted to predict the $f(\varphi_S)$ of composite pastes with CSA as solute. The relative viscosity of composite paste with different PC and CSA contents are shown in **Table 4** and **Table 5**. From the transverse view, when the φ_S is the same, the relative viscosity of different PC volume fraction pastes has little difference. In other words, in the prediction of $f(\varphi_S)$, the value of $f(\varphi_S)$ is only related to φ_S, but not to $\varphi_{C/W}$. This is consistent with the original assumption in predicting viscosity that firstly predict the viscosity of PC-H_2O system, and then predict the viscosity of PC-CSA-H_2O paste. The average relative viscosity of 5 groups under the same φ_S is taken as $f(\varphi_S)$, and the above four models are used to fit the relationship between $f(\varphi_S)$ and φ_S (shown in **Fig. 10**). It can be seen that whether at 5 min or 60 min, Einstein model can well characterize the relationship between $f(\varphi_S)$ and φ_S when taking into account the water film thickness. Based on the original data, the relative viscosity at 5 min and 60 min can be predicted by Eq. (21) and Eq. (22):

5 min:

$$f(\varphi_S) = 1 + 5.1288 * \varphi_S \quad (21)$$

60 min:

$$f(\varphi_S) = 1 + 6.8008 * \varphi_S \quad (22)$$

3.2.4 Prediction results and accuracy

After getting the function expression of $f(\varphi_{C/W})$ and $f(\varphi_S)$, the prediction model of η_{min} can be calculated. By substituting the expressions of $f(\varphi_{C/W})$ and $f(\varphi_S)$ at different resting time into Eq. (5)

and Eq. (6), the viscosity prediction equations of PC-CSA pastes at 5 min and 60 min are obtained respectively:

5 min:

$$\eta = 0.000936*[(0.097*(0.9144-\varphi_{C/W})]^{-2}*(1+5.1288*\varphi_S) \quad (23)$$

60 min:

$$\eta = 0.000936*[(0.0689*(1.0377-\varphi_{C/W})]^{-2}*(1+6.8008*\varphi_S) \quad (24)$$

In order to evaluate the prediction results of the above two equations, R^2 is used here to characterize the accuracy as well. As can be seen in **Fig. 11**, the R^2 of 60 min is lower than that of 5 min, indicating the prediction accuracy of η_{min} at 5 min is higher than that at 60 min. Based on the experimental results of viscoelasticity, it can be found that there are large differences among the values of G', G'' and δ at 5 min and 60 min, showing their colloidal interactions of particles and microstructure are different. Yield stress and viscosity are two common rheological parameters for fresh cement paste. The yield stress of cement paste comes from the microscopic network structure formed by colloidal interaction [38, 39]. When the cement paste is in a static state, colloidal flocculation and cement hydration bond (i.e. C-S-H bridge) will form microstructure in paste, thus increasing the yield stress [39]. Viscosity refers to the resistance to flow and it can characterize the deformation speed of cement paste. Unlike yield stress, viscosity is more related to energy dissipation during flow behavior [40], i.e., volume fraction of particles [41, 42], Specific surface area [43], packing effect [44] and friction effect [45]. With the extension of resting time, the viscoelastic properties and factors such as flocculation network structure and colloidal attractive forces related to yield stress of cement mixes change. These variations do not significantly influence the relationship between particle volume fractions and

viscosity at different resting time (As can be seen from Eq. (23) and Eq. (24), the form of two equations is still the same and the parameters are close to each other), but decrease the R^2 from 0.9794 to 0.9639. The change of viscoelasticity at 5 min and 60 min due to the formation of flocculation structure and hydration products is the main reason for the decline of viscosity prediction accuracy. Therefore, it is reasonable to believe that an appropriate prediction time is 5 min if the particles volume fraction is used to predict the η_{min} of PC-CSA pastes.

4 Conclusions

(1) With the increase of shear rate, PC-CSA pastes under different mix proportions show shear thinning behavior first and then shear thickening, and there is a η_{min} in each paste during the whole shear process. Higher PC and CSA particles volume fraction cause a larger η_{min}.

(2) All PC-CSA pastes have linear viscoelastic regions. When G' or G'' is less than critical strain, they can keep constant in a certain range. With the increase of $f(\varphi_{C/W})$ and $f(\varphi_S)$, the value of G' and G'' corresponding to the critical strain increases, and the critical strain and flow point strain also increase. With the prolongation of resting time, the phase angles of composite pastes change significantly at 5min and 60 min, demonstrating that the viscoelasticity is in a trend of dynamic variation.

(3) Einstein model and Krieger and Dougherty model are used to describe the functional expressions of $f(\varphi_{C/W})$ and $f(\varphi_S)$ respectively. The relationships between η_{min}, $\varphi_{C/W}$ and φ_S at 5 min and 60 min are obtained under the condition of considering the water film thickness. The R^2 values of the prediction models at two resting time are both high, which proves the accuracy of calculated results. By comparing the results it can be found that the prediction model at 5 min has higher accuracy than that of 60 min. Besides the particles volume fraction, the formation of flocs and

hydrated products also have a certain impact on the rheological properties with the extension of resting time.

Declaration of competing interest

The authors declare that they have no known competing financial interests or personal relationships that could have appeared to influence the work reported in this paper.

Acknowledgements

This work was financially supported by China Scholarship Council (grant number: 202006370082).

References

[1] G. Zhang, Y. Yang, H. Yang, H. Li, Calcium sulphoaluminate cement used as mineral accelerator to improve the property of Portland cement at sub-zero temperature. Cem. Concr. Compos. 106 (2020) 103452, https://doi.org/10.1016/j.cemconcomp.2019.103452.

[2] S. Allevi, M. Marchi, F. Scotti, S. Bertini, C. Cosentino, Hydration of calcium sulphoaluminate clinker with additions of different calcium sulphate sources, Mater. Struct. 49 (1-2) (2016) 453-466, https://doi.org./10.1617/s11527-014-0510-5.

[3] M. Singh, P.C. Kapur, Pradip, Preparation of calcium sulphoaluminate cement using fertiliser plant wastes, J. Hazard. Mater. 157 (1) (2008) 106-113, https://doi.org/10.1016/j.jhazmat.2007.12.117.

[4] Juenger, M. C. G., Winnefeld, F., Provis, J. L., & Ideker, J. H. (2011). Advances in alternative cementitious binders. Cem. Concr. Res. 41(12), 1232-1243, https://doi.org/10.1016/j.cemconres.2010.11.012.

[5] J. Beretka, R.Cioffi, M. Marroccoli, G.L. Valenti, Energy-saving cements obtained from chemical gypsum and other industrial wastes, Waste Manage. 16 (1-3) (1996) 231-235, https://doi.org/10.1016/S0956-053X(96)00046-3.

[6] J. Berekta, B. De Vito, L. Santoro, N. Sherman, G.L. Valenti, Hydraulic behavior of calcium sulphoaluminate-based cements derived from industrial process wastes, Cem. Concr. Res. 23 (5) (1993) 1205–1214, https://doi.org/10.1016/0008-8846(93)90181-8.

[7] J. Zhang, G. Ke, Y. Liu, Experimental study on shrinkage reduction of calcium sulphoaluminate cement concrete with addition of pre-wetted lightweight aggregate, Constr. Build. Mater. 253 (2020) 119149, https://doi.org/10.1016/j.conbuildmat.2020.119149.

[8] D. Gastaldi, F. Canonico, L. Capelli, M. Bianchi, M. Pace, A. Telesca, Hydraulic behaviour of calcium sulfphoaluminate cement alone and in mixture with Portland cement, Proc. 13th Int. Congr. Chem. Cem., Madrid, Spain, 2011, 412.

[9] L. Pelletier, F. Winnefeld, B. Lothenbach, The ternary system Portland cement–calcium sulphoaluminate clinker–anhydrite: hydration mechanism and mortar properties, Cem. Concr. Compos. 32 (7) (2010) 497-507, https://doi.org./10.1016/j.cemconcomp.2010. 03.010.

[10] P.M. Wang, N. Li, L.L. Xu, Hydration evolution and compressive strength of calcium sulphoaluminate cement constantly cured over the temperature range of 0 to 80 degrees C, Cem. Concr. Res. 100 (2017) 203-213, https://doi.org./10.1016/j.cemconres.2017.05.025.

[11] Y. Shen, J.S. Qian, J.Q. Chai, Y.Y. Fan, Calcium sulphoaluminate cements made with phosphogypsum: Production issues and material properties, Cem. Concr. Compos. 48 (2014) 67-74, https://doi.org./10.1016/j.cemconcomp.2014.01.009.

[12] G.X. Li, J.J. Zhang, Z.P. Song, C. Shi, A. Zhang, Improvement of workability and early strength of calcium sulphoaluminate cement at various temperature by chemical admixtures, Constr. Build. Mater. 160 (2018) 427-439, https://doi.org./ 10.1016/j.conbuildmat.2017.11.076.

[13] G. Zhang, G.X. Li, Y.C. Li, Effects of superplasticizers and retarders on the fluidity and strength of sulphoaluminate cement, Constr. Build. Mater. 126 (2016) 44-54, https://doi.org./ 10.1016/j.conbuildmat.2016.09.019.

[14] X.H. Fu, C.X. Yang, Z.M. Liu, W.H. Tao, W.P. Hou, X.Q. Wu, Studies on effects of activators on properties and mechanism of hydration of sulphoaluminate cement, Cem. Concr. Res. 33(3) (2003) 317-324, https://doi.org./10.1016/S0008-8846(02)00954-7.

[15] L. Ting, W. Qiang, S.Y. Zhuang, Effects of ultra-fine ground granulated blast-furnace slag on initial setting time, fluidity and rheological properties of cement pastes, Powder Technol. 345, (2019) 54-63, https://doi.org/10.1016/j.powtec.2018.12.094.

[16] S. Nunes, P.M. Oliveira, J.S. Coutinho, J. Figueiras, Rheological characterization of SCC mortars and pastes with changes induced by cement delivery, Cem. Concr. Compos. 33 (1) (2011) 103-115, https://doi.org./10.1016/j.cemconcomp.2010.09.019.

382 [17] G. Sant, C.F. Ferraris, J. Weiss, Rheological properties of cement pastes: A discussion of
383 structure formation and mechanical property development, Cem. Concr. Res. 38 (11) (2008) 1286-
384 1296, https://doi.org/10.1016/j.cemconres.2008.06.008.
385 [18] H. Yang, C.R. Lu, G.X. Mei, Shear-Thickening Behavior of Cement Pastes under Combined
386 Effects of Mineral Admixture and Time, J. Mater. Civ. Eng. 30 (2) (2018) 04017282,
387 https://doi.org/10.1061/(ASCE)MT.1943-5533.0002123.
388 [19] G.J. Ke, J. Zhang, S.X. Xie, T.C. Pei, Rheological behavior of calcium sulfoaluminate cement
389 paste with supplementary cementitious materials, Constr. Build. Mater. 243 (2020) 118234,
390 https://doi.org./10.1016/j.conbuildmat.2020.118234.
391 [20] Q. Yuan, X. Lu, K.H. Khayat, D. Feys, C.J. Shi, Small amplitude oscillatory shear technique to
392 evaluate structural build-up of cement paste, Mater. Struct. 50 (2) (2017) 112,
393 https://doi.org/10.1617/s11527-016-0978-2.
394 [21] J.T. Kolawole, R. Combrinck, W.P. Boshoff, Rheo-viscoelastic behaviour of fresh cement-
395 based materials: Cement paste, mortar and concrete, Constr. Build. Mater. 248 (2020) 118667,
396 https://doi.org./10.1016/j.conbuildmat.2020.118667.
397 [22] Y. Liu, C.J. Shi, D.W. Jiao, X.P. An, Rheological Properties, Models and Measurements for
398 Fresh Cementitious Materials—A Short Review, J. Chin. Ceram. Soc, 45 (2017) 708-716.
399 https://doi.org/10.14062/j.issn.0454-5648.2017.05.17. (in Chinese)
400 [23] H.Y. Cheng, S.C. Wu, H. Li, X.Q. Zhang, Influence of time and temperature on rheology and
401 flow performance of cemented paste backfill, Constr. Build. Mater. 231 (2020) 117117,
402 https://doi.org./10.1016/j.conbuildmat.2019.117117.
403 [24] M.X. Chen, L.B. Li, Y. Zheng, P.Q. Zhao, L.C. Lu, X. Cheng, Rheological and mechanical
404 properties of admixtures modified 3D printing sulphoaluminate cementitious materials, Constr.
405 Build. Mater. 189 (2018) 601-611, https://doi.org./10.1016/j.conbuildmat.2018.09.037.
406 [25] J.C. Yu, J.S. Qian, J.Y. Tang, Z.W. Ji, Y.R. Fan, Effect of ettringite seed crystals on the
407 properties of calcium sulphoaluminate cement, Constr. Build. Mater. 207 (2019) 249-257,
408 https://doi.org./10.1016/j.conbuildmat.2019.02.130.
409 [26] J. Ouyang, B.G. Han, G.Z. Chen, L.Z. Zhao, J.P. Ou, A viscosity prediction model for cement
410 paste with nano-SiO2 particles, Constr. Build. Mater. 185 (2018) 293-301,
411 https://doi.org./10.1016/j.conbuildmat.2018.07.070.

412 [27] N. A. Tregger, M. E. Pakula, S. P. Shah, Influence of clays on the rheology of cement
413 pastes. Cement and concrete research, 40 (3) (2010) 384-391
414 https://doi.org/10.1016/j.cemconres.2009.11.001.
415 [28] K. Sobolev, I.F. Vivian, R. Saha, N.M. Wasiuddin, N.E. Saltibus, The effect of fly ash on the
416 rheological properties of bituminous materials, Fuel, 116 (2014) 471-477, https://doi.org./
417 10.1016/j.fuel.2013.07.123.
418 [29] I. Mehdipour, K. H. Khayat, Understanding the role of particle packing characteristics in rheo-
419 physical properties of cementitious suspensions: A literature review, Constr. Build. Mater. 161
420 (2018) 340-353 https://doi.org/10.1016/j.conbuildmat.2017.11.147.
421 [30] I.M. Krieger, T.J. Dougherty, A mechanism for non-Newtonian flow in suspensions of rigid
422 spheres, J. Rheol. 3 (1) (1959) 137–152.
423 [31] D. Liu, Particle packing and rheological property of highly-concentrated ceramic suspensions:
424 phi(m) determination and viscosity prediction, J. Mater. Sci. 35 (21) (2000) 5503–5507, https://
425 doi.org/10.1023/A:1004885432221.
426 [32] A. Einstein, Investigation on the Theory of Brownian Movement, Dover Publications, New
427 York, 1956.
428 [33] G.K. Batchelor, The effect of Brownian motion on the bulk stress in a suspension of spherical
429 particles, J. Fluid Mech. 83 (01) (1977) 97–117. https:// doi.org/10.1017/S0022112077001062.
430 [34] H.C. Brinkman, The viscosity of concentrated suspensions and solutions, J. Chem. Phys. 20 (4)
431 (1952) 571-571. https:// doi.org/10.1063/1.1700493.
432 [35] J. Qiu, Z. Guo, L. Yang, H. Jiang, Y. Zhao, Effects of packing density and water film thickness
433 on the fluidity behaviour of cemented paste backfill, Powder Technol. 359 (2020) 27-35.
434 https://doi.org/10.1016/j.powtec.2019.10.046.
435 [36] J.J. Chen, B.H. Li, P.L. Ng, A.K.H. Kwan, Adding granite polishing waste as sand replacement
436 to improve packing density, rheology, strength and impermeability of mortar, Powder Technol. 364,
437 (2020) 404-415. https://doi.org/10.1016/j.powtec.2020.02.012.
438 [37] G. Marchetti, E. F. Irassar, V. F. Rahhal, Effects of packing density and water film thickness on
439 fresh and hardened properties of ternary cement pastes. Adv. Cem. Res. 32 (10) (2020) 444-455.
440 https://doi.org/10.1680/jadcr.18.00133.
441 [38] B.I. Choi, J.H. Kim, T.Y. Shin, Rheological model selection and a general model for evaluating

the viscosity and microstructure of a highly-concentrated cement suspension, Cem. Concr. Res. 123 (2019) 105775, https://doi.org/10.1016/j.cemconres.2019.05.020.

[39] N. Roussel, H. Bessaies-Bey, S. Kawashima, D. Marchon, K. Vasilic, R. Wolfs, Recent advances on yield stress and elasticity of fresh cement-based materials, Cem. Concr. Res. 124 (2019) 105798, https://doi.org./10.1016/j.cemconres.2019.105798.

[40] Q.Q. Zhang, J.Z. Liu, J.P. Liu, F.Y. Han, W. Lin, Effect of superplasticizers on apparent viscosity of cement-based material with a low water–binder ratio, J. Mater. Civ. Eng. 28 (9) (2016) 04016085, https://doi.org./10.1061/(ASCE)MT.1943-5533.0001590.

[41] A. Ilyushechkin, A. Kondratiev, Viscosity of slags with solids: The effect of solids morphology and concentration, J. Rheol. 63 (5) (2019)719-733, https://doi.org./10. 1122/1.5095968.

[42] A. Yahia, Effect of solid concentration and shear rate on shear-thickening response of high-performance cement suspensions, Constr. Build. Mater. 53 (2014) 517-521, https://doi.org./10.1016/j.conbuildmat.2013.10.078.

[43] A. Mezhov, U. Pott, D. Stephan, K. Kovler, Influence of mechanical activation of fly ash in presence of polynaphthalene sulfonate superplasticizer on rheology and hydration kinetics of cement–fly ash pastes, Constr. Build. Mater. 210 (2019) 380-390, https://doi.org./ 10.1016/j.conbuildmat.2019.03.190.

[44] X.J. Deng, B. Klein, D.J. Hallbom, B. de Wit, J.X. Zhang, Influence of particle size on the basic and time-dependent rheological behaviors of cemented paste backfill, J. Mater. Eng. Perform. 27 (7) (2018) 3478-3487, https://doi.org./10.1007/s11665-018- 3467-7.

[45] T. Yang, H.J. Zhu, Z.H. Zhang, X. Gao, C.S. Zhang, Q.S. Wu, Effect of fly ash microsphere on the rheology and microstructure of alkali-activated fly ash/slag pastes, Cem. Concr. Res. 109 (2018) 198-207, https://doi.org./10.1016/j.cemconres.2018.04.008.

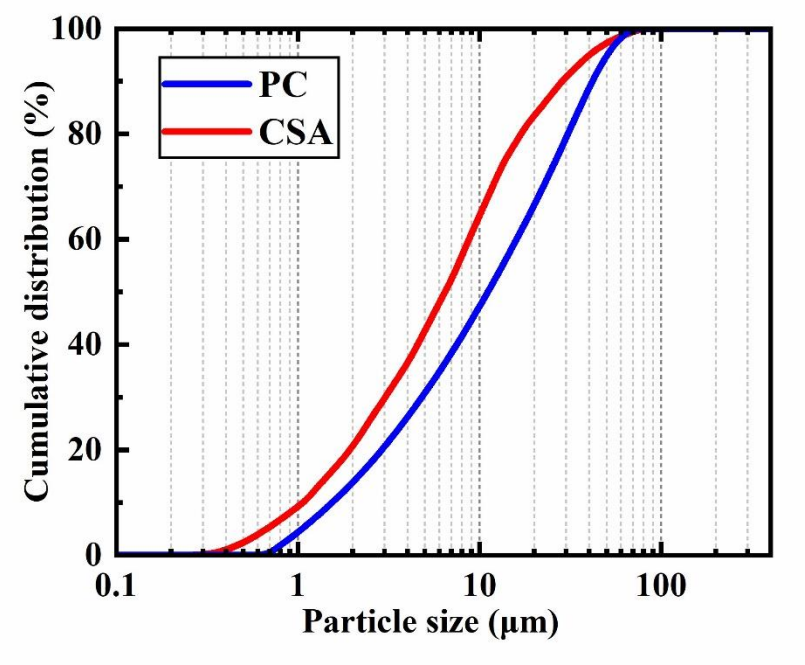

Fig. 1 Particle size distributions of PC and CSA

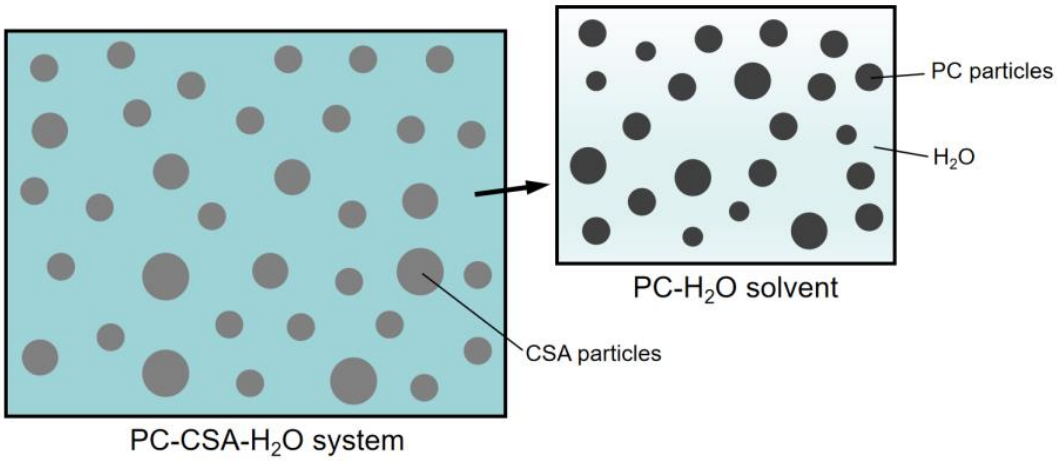

Fig. 2 An illustration of PC-CSA-H_2O system

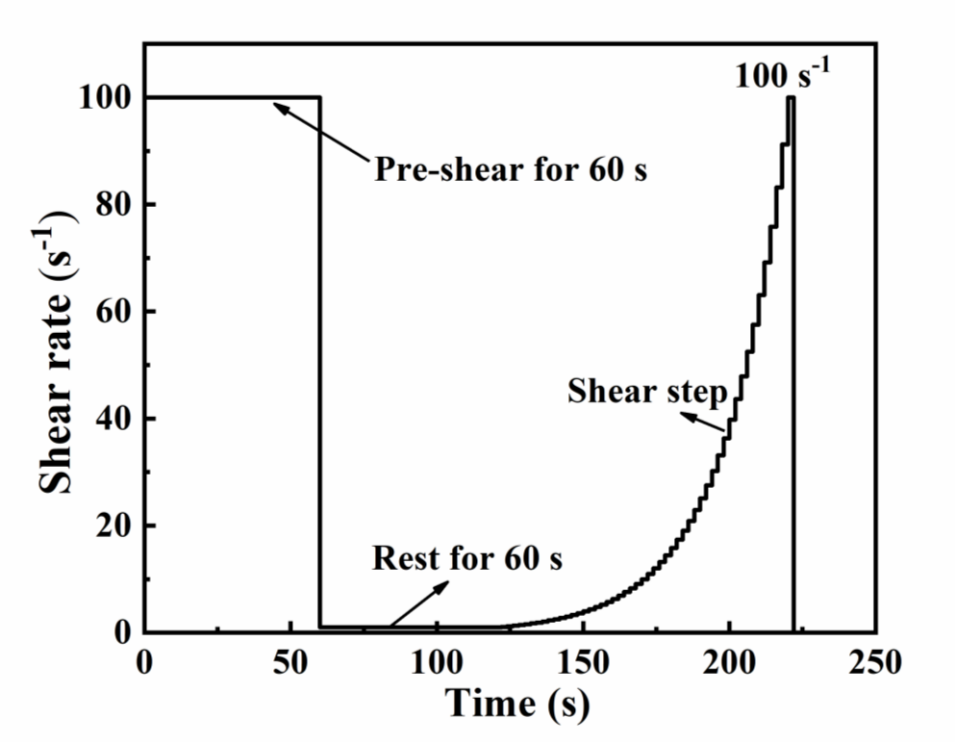

Fig. 3 Test protocol for dynamic rheological test

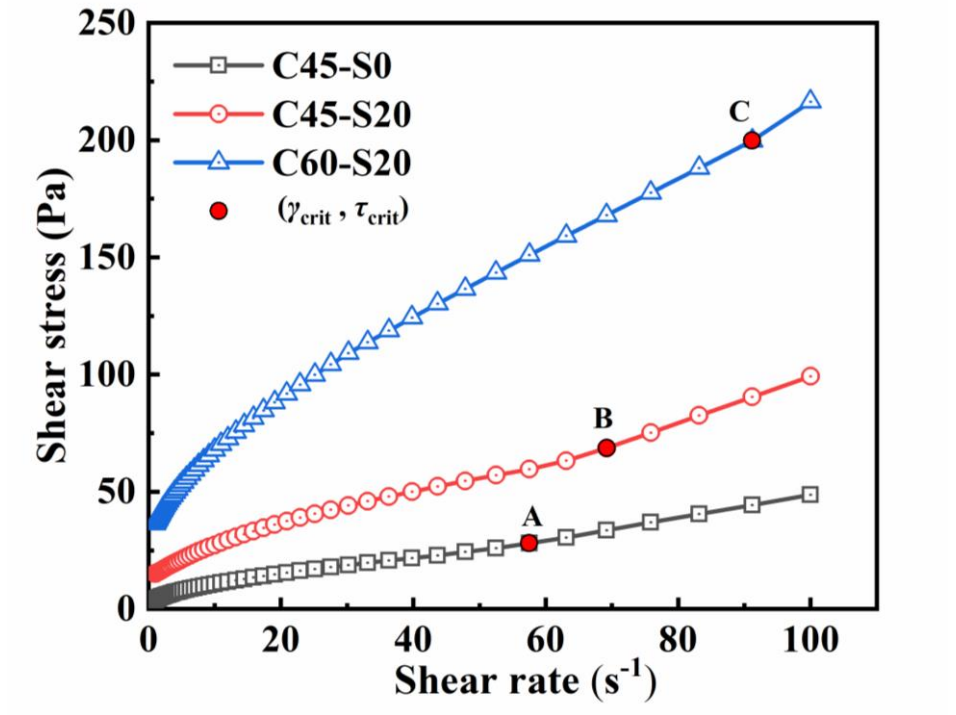

(a) Shear rate *vs.* shear stress

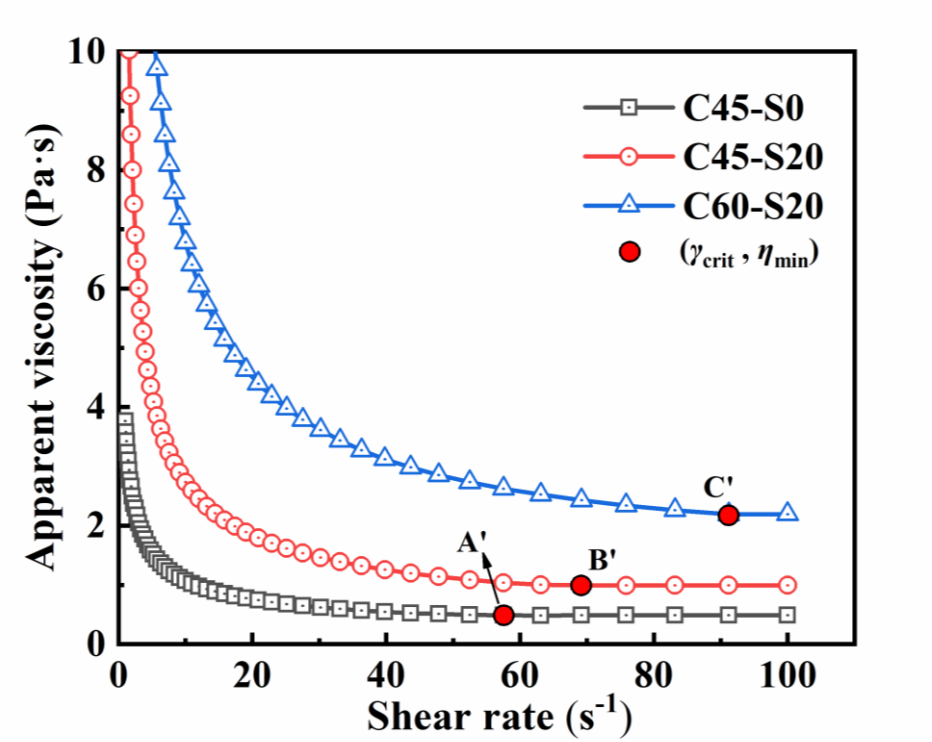

(b) Shear rate *vs.* apparent viscosity

Fig. 4 Rheological curves of PC-CSA pastes

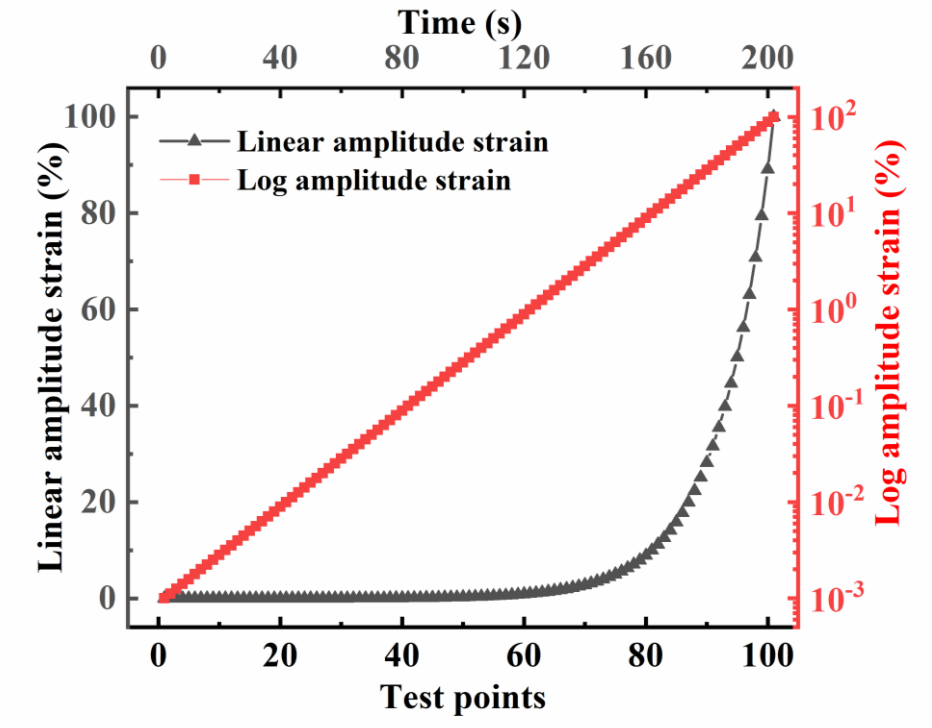

Fig. 5 Test protocol for amplitude sweep

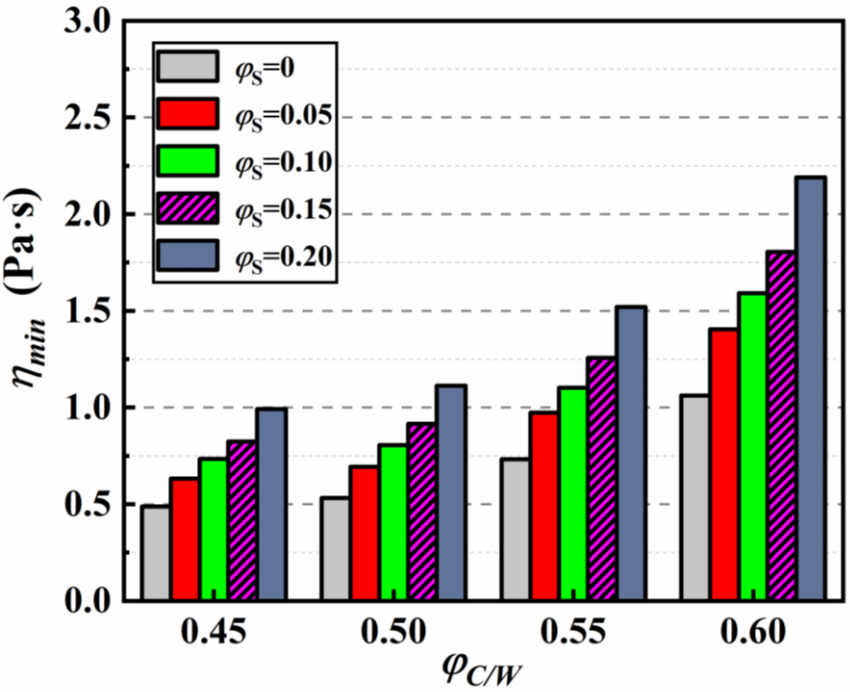

(a) 5 min

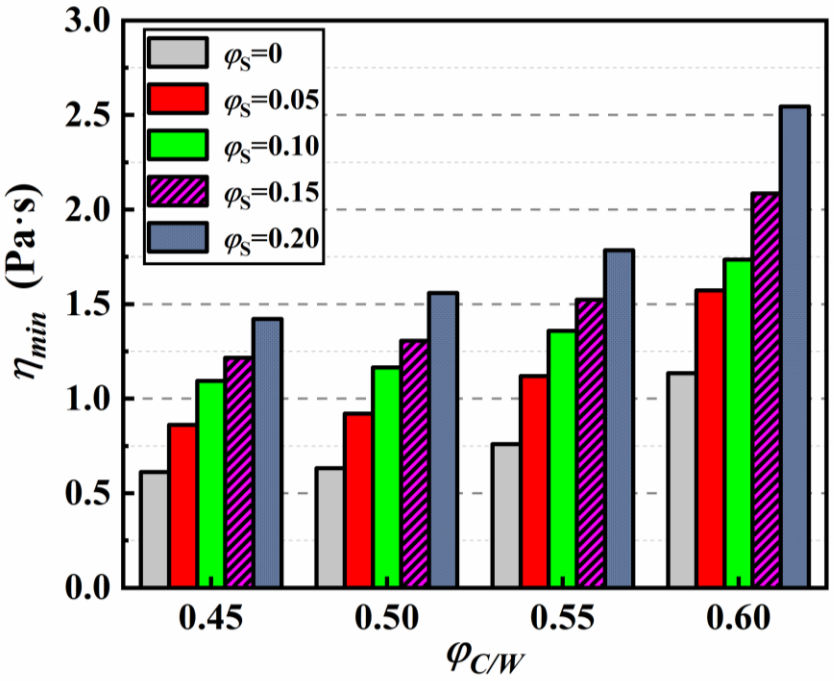

(b) 60 min

Fig. 6 The minimum apparent viscosities of PC-CSA pastes

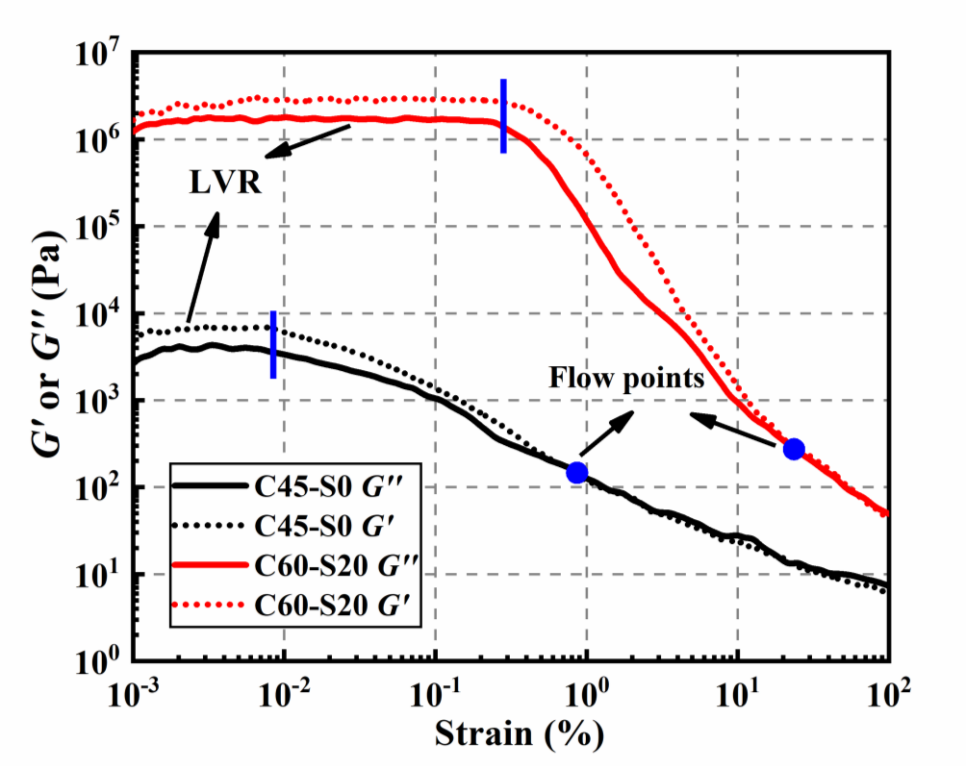

Fig. 7 Typical amplitude sweep curves of PC-CSA pastes

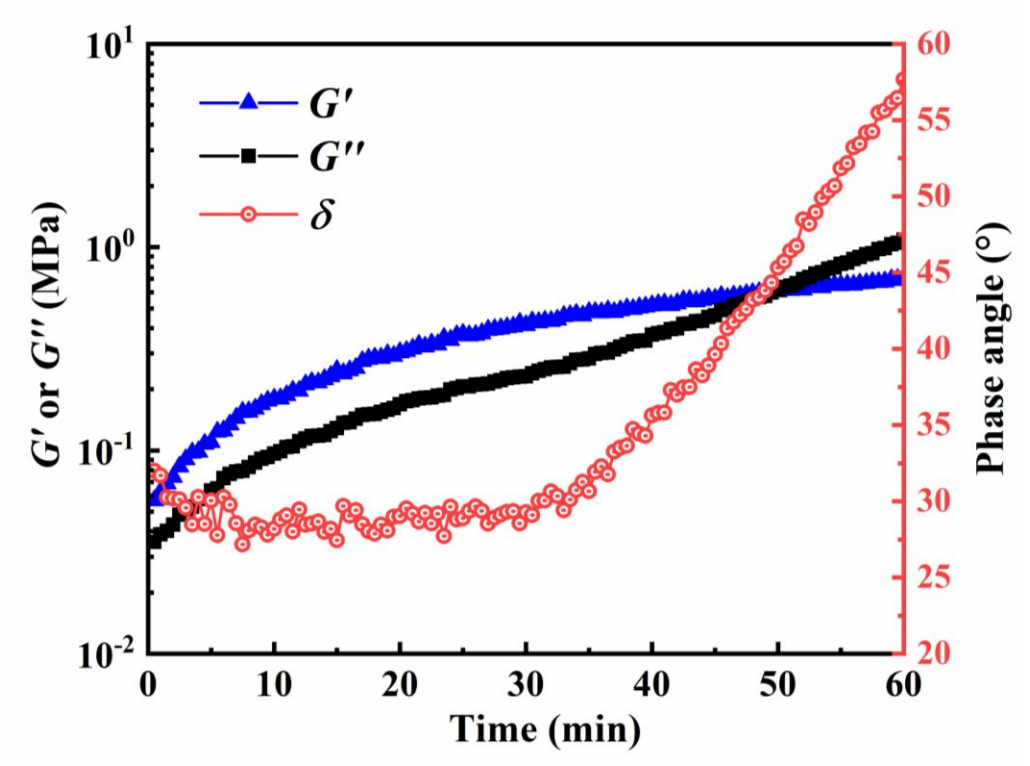

(a) C45-S0

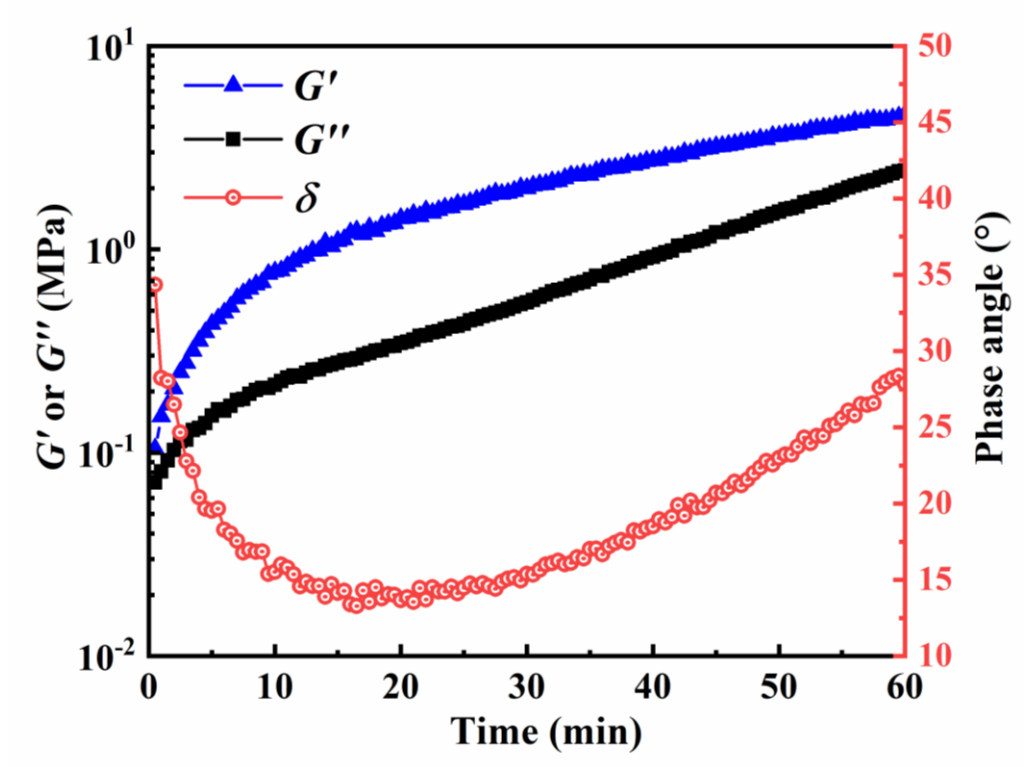

(b) C45-S20

Fig. 8 Evolution of G', G'' and δ with time at a frequency of 1 Hz and a strain amplitude of 10^{-4}

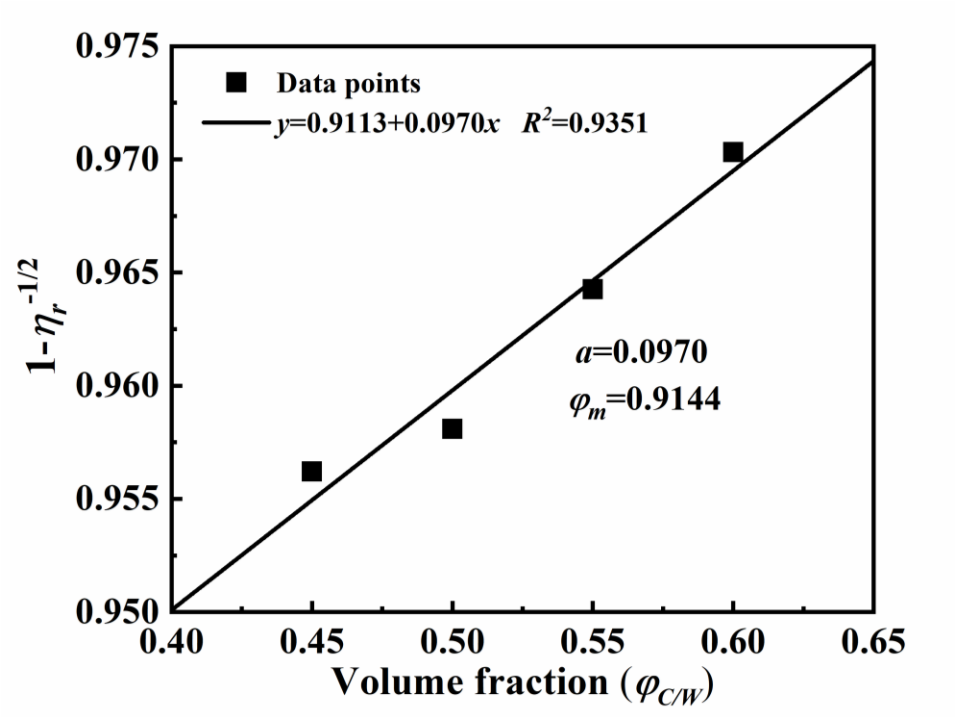

(a) 5min

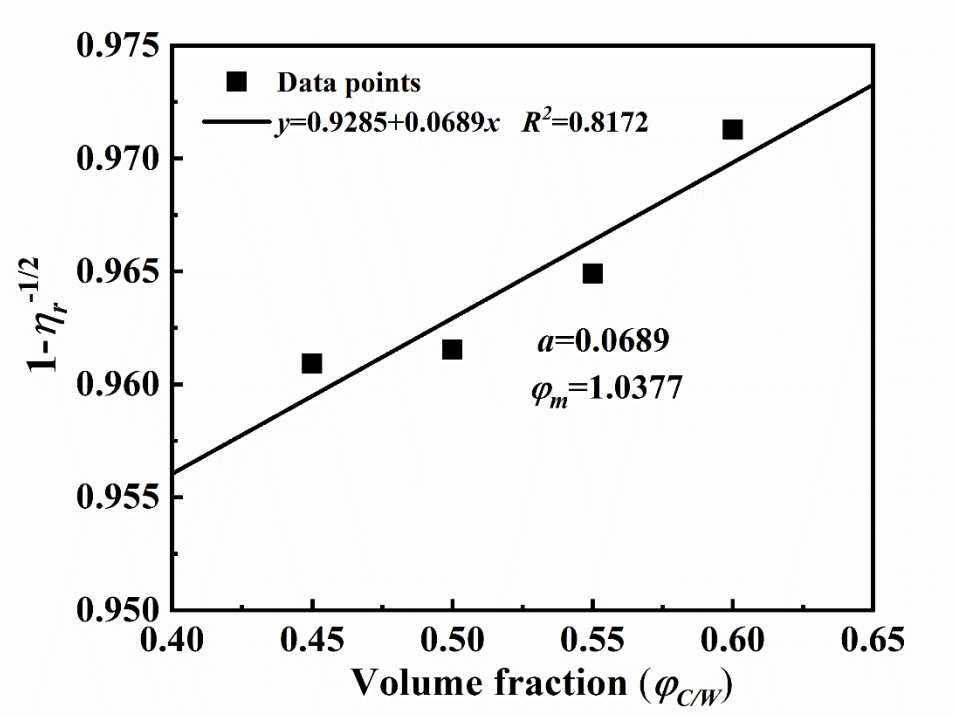

(b) 60 min

Fig. 9 The values of a and φ_m calculated by the linear relationship between $1-\eta_r^{-1/2}$ and φ when R^2 reaches the maximum

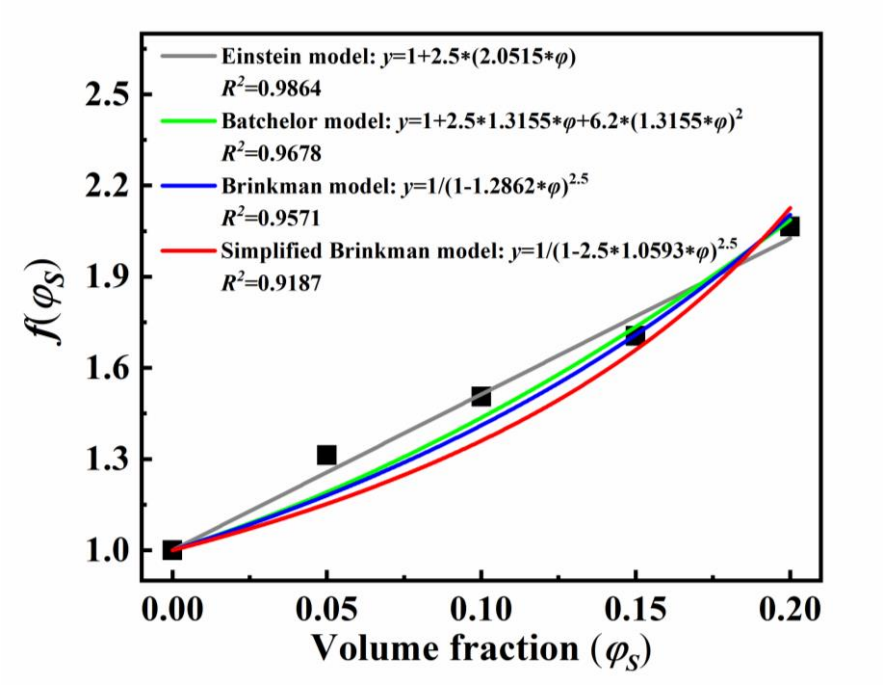

505

506 (a) 5 min

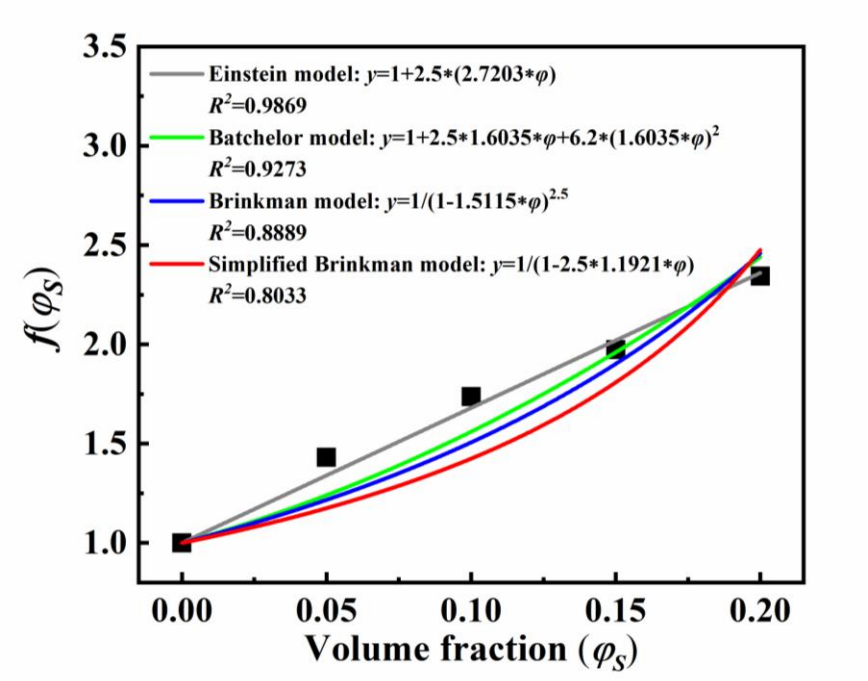

507

508 (b) 60 min

509 **Fig. 10** The relationships between $f(\varphi_S)$ and φ_S fitted by different prediction models

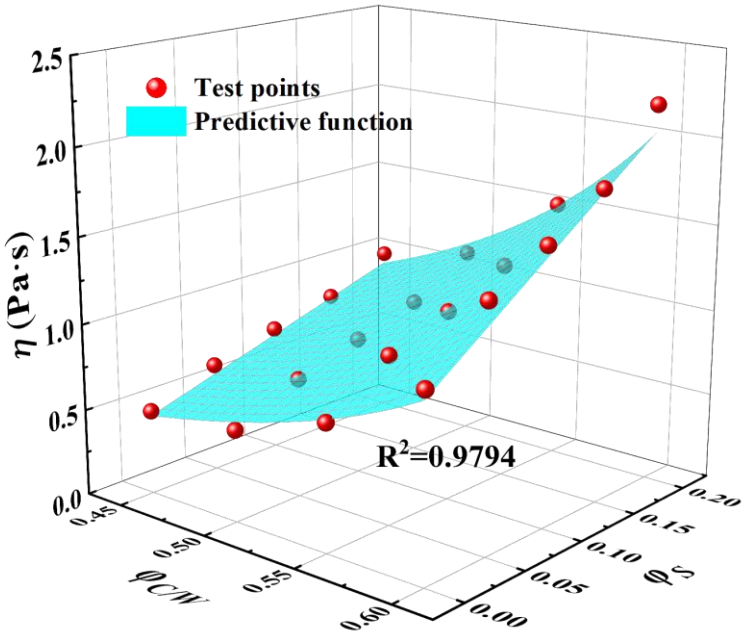

(a) 5 min

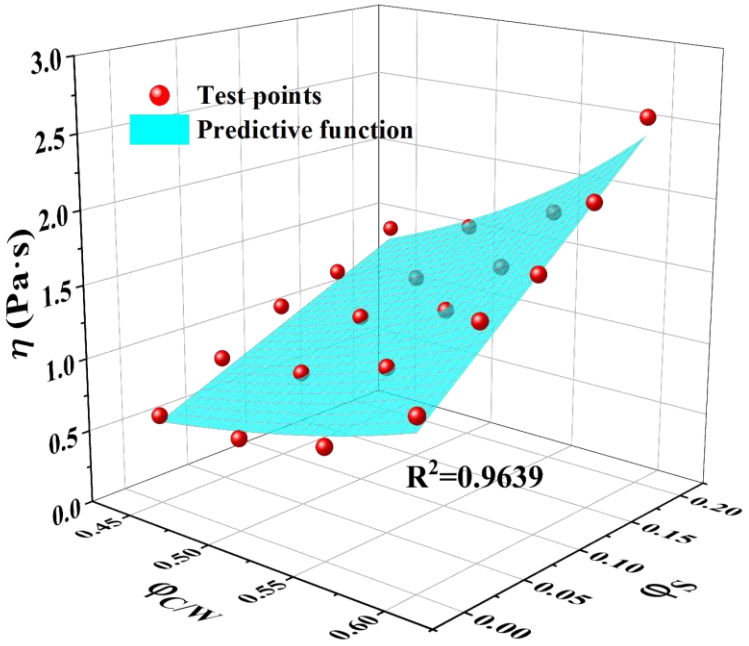

(b) 60 min

Fig. 11 The prediction results of PC-CSA pastes at different resting time

Table 1 Physical properties and chemical compositions of PC and CSA

Raw materials	Composition (wt.%)						Ignition loss (%)	Density (g/cm^3)
	CaO	Al_2O_3	SiO_2	Fe_2O_3	SO_3	MgO		
PC	62.26	7.31	20.76	3.25	2.81	2.91	2.10	3.15
CSA	46.79	22.83	11.72	1.50	12.09	1.72	1.33	2.80

Table 2 Mixture proportions of PC-CSA systems

Sample	Volume ratio (%)			Mass ratio (%)			*W/B*
	$\varphi_C+\varphi_W$	$\varphi_C/(\varphi_C+\varphi_W)$	φ_S	PC	CSA	H_2O	
C45-S0	100	45	0	141.8	0	55	0.388
C45-S5	95	45	5	134.7	14	52.3	0.351
C45-S10	90	45	10	127.6	28	49.5	0.318
C45-S15	85	45	15	120.5	42	46.8	0.288
C45-S20	80	45	20	113.4	56	44	0.260
C50-S0	100	50	0	157.5	0	50	0.317
C50-S5	95	50	5	149.6	14	47.5	0.290
C50-S10	90	50	10	141.8	28	45	0.265
C50-S15	85	50	15	133.9	42	42.5	0.242
C50-S20	80	50	20	126	56	40	0.220
C55-S0	100	55	0	173.3	0	45	0.260
C55-S5	95	55	5	164.6	14	42.8	0.239
C55-S10	90	55	10	155.9	28	40.5	0.220
C55-S15	85	55	15	147.3	42	38.3	0.202
C55-S20	80	55	20	138.6	56	36	0.185
C60-S0	100	60	0	189	0	40	0.212
C60-S5	95	60	5	179.6	14	38	0.196
C60-S10	90	60	10	170.1	28	36	0.182
C60-S15	85	60	15	160.7	42	34	0.168
C60-S20	80	60	20	151.2	56	32	0.154

532 **Table 3** Critical strain, G', G'' and flow point strain

Sample	Critical strain (%)	G' at critical strain (Pa)	G'' at critical strain (Pa)	Flow point strain (%)
C45-S0	0.0079	6,902	4,026	0.7943
C45-S20	0.0158	82,190	63,910	2.512
C60-S0	0.0251	315,800	228,200	3.545
C60-S20	0.1995	2,812,000	1,619,000	19.95

533

534 **Table 4** The relative viscosity of PC-CSA paste at 5 min ($f(\varphi_S)$)

φ_S	$\varphi_{C/W}$				Average value
	45	50	55	60	
0	1.000	1.000	1.000	1.000	1.000
5	1.298	1.302	1.328	1.323	1.312
10	1.504	1.512	1.505	1.498	1.505
15	1.688	1.718	1.716	1.699	1.705
20	2.032	2.088	2.074	2.061	2.064

535

536 **Table 5** The relative viscosity of PC-CSA paste at 60 min ($f(\varphi_S)$)

φ_S	$\varphi_{C/W}$				Average value
	45	50	55	60	
0	1.000	1.000	1.000	1.000	1.000
5	1.407	1.454	1.474	1.386	1.431
10	1.785	1.841	1.788	1.530	1.736
15	1.987	2.065	2.005	1.838	1.974
20	2.321	2.462	2.350	2.244	2.344

537

538